A database of aerosols and gases coefficients for VIS-NIR radiative transfer in the Solar System planetary atmospheres.

F. Oliva [a,*], E. D'Aversa [a], G. L. Liberti [b], G. Sindoni [a], F. Altieri [a], E. Castelli [b]

[a]Institute for Space Astrophysics and Planetology, INAF, Via del Fosso del Cavaliere 100, 00133 Rome, Italy

[b]Institute of Atmospheric Sciences and Climate, ISAC-CNR, Via Piero Gobetti 101, 40129, Bologna, Italy

Abstract

Radiative transfer (RT) modelling of planetary atmospheres allows to obtain extremely valuable information about these environments. The computation of optical properties of the aerosols and gases, that is heavily time consuming, is always required as input for both forward models and inversion algorithms. We provide look up tables for these coefficients, ready to be ingested in RT solvers, in the visible and near infrared spectral ranges and covering the main species of the Solar System planets' atmospheres. Gases absorption coefficients have been computed with the line-by-line approach from the HITRAN 2012 spectral database and an improved method to interpolate them is suggested. Aerosols single scattering properties have been computed using the Mie and Rayleigh models for a set of selected species relevant for planetary atmospheres. Optimization in terms of tabulated wavelengths and maximum number of Legendre polynomial expansion terms has been performed for each species.

Keywords: Radiative transfer
Spectroscopy
Aerosols optical constants
Gases absorption coefficients
Atmospheres, composition

1. Introduction

The modelling of radiative transfer (RT) is the main tool for interpreting remote sensing observations of planetary atmospheres (Haus and Arnold, 2010; Cess and Ramanathan, 1972; Määttänen et al., 2009; Geminale et al., 2015; Oliva et al., 2018; Karkoschka and Tomasko, 2005; Pérez-Hoyos et al., 2005; Oliva et al., 2016; Zhang et al., 2013; Sindoni et al., 2017; Chance and

* Corresponding Author. Tel: +39 06 45488201

E-mail address: (fabrizio.oliva@iaps.inaf.it)

Martin, 2017). Theories and models implementations in this field are developing since decades, growing in accuracy to keep up with the increasing resolution of measurements in laboratory and from space. Remote sensing in the visible (VIS) and near-infrared (NIR) spectral range is widely used on almost all planetary exploration missions of current generation to probe composition (Titov et al., 2007; Poulet et al., 2003; Fletcher et al., 2009), vertical structure (Sromovsky et al., 2013; Pérez-Hoyos et al., 2012), thermodynamics (Fletcher et al., 2015; Colaprete and Toon, 2000), and interactions of a planetary atmosphere (Brackett et al., 1995). Non-gaseous constituents of atmospheres are often composed by particulates with typical sizes ranging from nanometre to micrometres, i.e. of the same orders of magnitude of the wavelength of VIS and NIR light (Karkoschka and Tomasko, 2005; Oliva et al., 2018; Sindoni et al., 2017). This, along with the presence of important absorption complexes of the most diffuse molecules, makes this spectral range preferred for studying the spatial and temporal distribution of particulates and their microphysical properties (Oliva et al., 2018; Sindoni et al., 2017; Oliva et al., 2016; Sromovsky et al., 2013, Roman et al., 2013).

The retrieval of physical quantities from observations is highly dependent on the accuracy of our modeling of light absorption and scattering processes taking place within the different atmospheric layers. Wavelength-dependent absorption and scattering coefficients (hereafter Optical Properties, OP) are commonly used to parameterize the propagation of the radiation through the atmosphere, as they can be evaluated separately for each gaseous and solid/liquid component in their own thermodynamic condition. Therefore, the OPs represent the bulk of the atmospheric models used for both forward and inverse RT computations. However, their evaluation with sufficient accuracy is often heavily time consuming, also because they have to be evaluated for all possible conditions of temperature, pressure, and composition expected in the probed atmospheric layers.

As far as the gases absorption is concerned, the most rigorous approach for computing absorption coefficients for any temperature and pressure is the line-by-line (LBL) one. It requires the calculation of the absorption distribution in frequency for each molecular roto-vibrational transition in a given spectral range, and allows taking into account several line broadening processes. Since the line broadening is the effect of several pressure- and temperature-dependent processes, the computational load of LBL is essentially related to the repeating evaluation of the line shape at least for each molecular line and different pressure, temperature, and mixing ratio values.

Several approximated methods have been proposed to speed up the computations. For example, band models have been developed in the past for parameterizing the variations of individual molecular absorption bands with pressure and temperature (e.g. Goody, 1952; Pierrot et al.,1999; Karkoschka and Tomasko, 2010), but they suffer strong limitations and low accuracy for atmospheric spectroscopic studies. The correlated-k technique (Goody and Yung, 1989), based on the statistical distribution of absorption coefficients within suitable spectral bins, demonstrated better performances in reproducing gaseous absorption for planetary atmospheres (Tsang et al., 1999; Irwin et al., 2008; West et al., 2010). However, it is strongly constrained in terms of spectral resolution, since computation cannot be done for intervals smaller than the initial bins, and the computational cost greatly increases when the bins become narrower and narrower.

In order to keep application flexibility in terms of spectral resolution for all extra-terrestrial planetary atmospheres, in this work we adopted the most rigorous LBL approach, linked with an interpolation scheme applied to a look up table (LUT) (Section 2.2). Attempts to interpolate LUTs of absorption coefficients have been made by other authors (e.g. Hill et al., 2013) with results that vary with the application field. In this framework, an improved interpolation method is tested.

As a starting point for defining the working ranges of OP databases we take into account the characteristics of existing VIS to NIR spectral datasets about different Solar System atmospheres taken by space-based spectrometers (see Table 1). These datasets include extremely valuable information about the atmospheres of Mars, Venus, Jupiter, Saturn, and Titan, that will be still under investigation for years. We take also into account features of future spectrometers like MAJIS (Piccioni et al., 2014), that will fly on board JUICE mission towards Jupiter's system. Hence, this choice drives the definition of the overall framework for evaluating optical properties. In fact, we only focused on the main absorbing molecules in planetary atmospheres, i.e. CH_4, CO_2, and H_2O, within the regimes of temperatures, pressures, and abundances probed by remote sensing in the considered planets. The spectral range for OP evaluation has been chosen to lie from 400 to 5500 nm, as a compromise between the ranges covered by selected spectrometers and those where molecular transitions and refraction indices are provided in literature.

Table 1: Definition of application fields for the considered datasets of OP ((a) Brown et al., 2004; (b) Bibring et al., 2005; (c) Piccioni et al., 2007; (d) Adriani et al. 2017; (e) Piccioni et al., 2014.)

Instrument	Spectral range [μm]	Spectral res [nm]	atmosphere	Main absorber	T range [K]	P max [bar]
Cassini VIMS (a)	0.35-5.1	7-17	Saturn	CH_4	80-220	~ 2.5
			Titan	CH_4	70-170	~ 1.4
MEx OMEGA (b)	0.35-5.1	13-20	Mars	CO_2 H_2O	150-270	~ 0.006
VEx VIRTIS (c)	0.3-5.0	1.8-9.8	Venus	CO_2	170-580	~ 90
Juno JIRAM (d)	2.0-5.0	9-12	Jupiter	CH_4	110-270	~ 2.5
Juice MAJIS (e)	0.4-5.7	2.3-6.6				

Another heavily time consuming operation in RT modelling is the estimation of Single Scattering Optical Properties (SSOPs) especially for particles that are relatively large compared to the wavelength at which the simulation is done. This issue is even more important in inversion algorithms that make use of real-time SSOPs computations. Radiative effects of condensate matter in planetary atmospheres cannot be neglected in the UV-NIR range. Retrieval of clouds and aerosols properties is a primary scientific subject to understand atmospheric processes (e.g. Oliva et al. 2016). Furthermore, surface studies take great advantage of the realistic representation of the condensate SSOPs, since it allows to remove the particulates contribution from the measurements (Brown, et al., 2014; Geminale et al., 2015). For these reasons, RT modeling should include a computationally efficient but accurate representation of the SSOPs. A way to achieve this is by storing the values of SSOP in pre-computed LUTs (Buehler et al., 2011; Vincent and Dudhia, 2017).

In this study we adopt the LUTs approach for both gas absorption coefficients (GAC) and particulates single scattering parameters (SSOP). In Section 2 we describe the techniques and approximations applied to the computation of GAC, whereas the Section 3 is devoted to SSOP description. Some application of LUTs to forward RT models and to spectral inversion are described in Section 4, and future perspective are illustrated in Section 5.

The full database, composed by several data files of very large dimensions (some gigabytes), is made available through ESA Planetary Science Archive (PSA) accessible at the website https://archives.esac.esa.int/psa/. Moreover, any specific request on the database can be made to the

118 authors.

119 2. Gaseous Absorption Coefficients

120 As abovementioned, we adopted the rigorous LBL approach to compute GACs for CH_4, CO_2,
121 and H_2O molecules, by taking advantage of the ARS RT libraries (Ignatiev et al., 2005). The
122 spectroscopic line parameters for these molecules have been taken from the HITRAN 2012
123 database (Rothman et al., 2013). This database lists a total amount of more than 800000 lines for
124 these molecules in the 400-5500 nm range.

125 *2.1. Absorption coefficients calculations*

126 Absorption coefficients for a given molecular species at wavenumber ν, pressure P,
127 temperature T, and mixing ratio χ is evaluated by LBL method as (Rothman et al., 1998):

128

$$129 \quad k(\nu,P,T) = \sum_{j=0}^{N} S_j(T_0) f_j(\nu,\nu_{0,j},P,T,\chi) \frac{Q(T_0)}{Q(T)} e^{-\frac{hc}{k_B}E_j\left(\frac{1}{T}-\frac{1}{T_0}\right)} (1-e^{-\frac{hc\nu_{0,j}}{k_B T}})/(1-e^{-\frac{hc\nu_{0,j}}{k_B T_0}}) \quad (1)$$

130

131 where the sum is extended to *N* molecular transitions of the species in a wide enough range, is the
132 line strength of j^{th} transition centered at wavenumber ν_0 and evaluated at a reference temperature T_0,
133 and f_j and E_j are the broadened line profile and the lower state energy of that transition respectively,
134 Q is the sum partition function, h, c, and k_B are the Planck constant, light speed, and Boltzmann
135 constant respectively.

136 It is evident from (1) that the spatial and temporal variations of gaseous absorption in a real
137 atmosphere are made complicated by to the highly non-linear dependence of these coefficients on
138 pressure, temperature and mixing ratio.

139 In the present work, we compute the absorption coefficients over a three-dimensional grid in
140 the space of parameters, defined by all the combinations of the values given in Table 3: 10 values of
141 pressures, logarithmically spaced between 5 bars and 10^{-6} bars, 10 values of temperatures, almost
142 linearly spaced between 70 K and 500 K, and 4 values of mixing ratio spanning several orders of
143 magnitude. Therefore, the total number of grid points amounts to 400 values for each wavelength.

144 We adopted the Voigt line profile to describe the broadened shape of individual molecular
145 lines, taking into account thermal and collisional broadening processes. The Lorentzian broadening
146 halfwidths (α) are calculated following Rothman et al. (1998):

147

$$148 \quad \alpha(P,T,\chi) = [\alpha_{air}(P_0,T_0)(1-\chi) + \alpha_{self}(P_0,T_0)\chi] \frac{P}{P_0} \left(\frac{T_0}{T}\right)^m \quad (2)$$

149

150 where α_{air} and α_{self} are the air- and self-broadening halfwidths, *m* is the exponent of temperature
151 dependence, P_0 and T_0 indicate reference values of pressure and temperature, and χ is the mixing
152 ratio of the species. Since α_{air} and α_{self} are not always available for the atmospheres of the Solar
153 System planets, we assumed the terrestrial values given in the HITRAN 2012 database.
154 Furthermore, isotopic fractionation is also kept on terrestrial values. Also the temperature
155 dependence of the Q functions has been taken from HITRAN 2012.

156 Since line shapes are computed over a same regularly-spaced wavenumbers grid for all lines,
157 we searched for an optimal wavenumber step allowing a trade-off between the accuracy on line

profile and the amount of data volume and calculation time. As a consequence, for each molecule we define spectral subintervals where grid steps can be kept constant, switching its value from 10^{-4} to 10^{-2} cm^{-1} based on lines density and broadening parameters (see Table 2). The errors we make with respect to a finer case (e.g. 10^{-5} cm^{-1}) are on average of the same order of the uncertainties due to our interpolation method (see Section 2.2 and Figure 2). For this reason, we discarded the possibility to use the finer case, since the enhancement in precision that it provides is not worth the increase in computational time and storage.

Table 2: spectral subinterval used for line shape computations. δ represents the wavenumber step adopted for line broadening calculations. Bold numbers indicate total values.

CH4			CO2			H2O		
Intervals (cm^{-1})	**Lines number**	**δ (cm^{-1})**	**Intervals (cm^{-1})**	**Lines number**	**δ (cm^{-1})**	**Intervals (cm^{-1})**	**Lines number**	**δ (cm^{-1})**
870-1250	29124	10^{-2}	782-1200	7869	10^{-2}	388-1030	92931	10^{-3}
1250-3060	176661	10^{-3}	1200-1850	66540	10^{-3}	1030-5999	106289	10^{-4}
3060-4890	96606	10^{-4}	1850-3470	170054	10^{-4}			
4890-6000	12853	$5x10^{-4}$	3470-3950	7383	10^{-3}			
			3950-5951	99576	10^{-4}			
870-6000	**315244**		**782-5951**	**351442**		**388-5999**	**199220**	

The wavenumber step used for shaping individual lines yields absorption coefficients guarantees the applicability of the LUTs to the analysis of the datasets in Table 1 (as well as of other similar datasets), being much narrower than the maximum resolution of these instruments (e.g. 1.8 nm/band of the visual channel of VIRTIS-M).

The HITRAN database also provides an estimation of uncertainties associated to each line parameter, which propagate non-linearly into the LBL calculations. We computed the uncertainties associated to absorption coefficients by using analytical derivatives of the line profile in the Lorentzian approximation. Average errors due to uncertainties on line strengths only, obtained in the spectral range under study in different P and T conditions, vary between 5% and 30% (e.g. left panel of Figure 2 for CH_4).

2.2. *Absorption coefficients interpolation*

We tested the application of several interpolation methods to the LUTs to check their usefulness in providing absorption coefficients for intermediate values of *P*, *T*, and χ These

methods include fits of the absorption coefficients or their logarithm, using different degree polynomials. These fits were performed on: P, T and χ; their logarithm; their inverse. The most performing method, that is more accurate in reproducing the values of exact calculations, relies on a three-steps procedure: 1) 7^{th} degree logarithmic polynomial fit with respect to P; 2) 7^{th} degree polynomial fit of the fit coefficients obtained in step 1 with respect to the inverse of *T*; 3) 2^{nd} degree polynomial fit of the fit coefficients from step 2 with respect to χ. We used a 7^{th} degree polynomial for steps 1) and 2) because lower degrees are not as precise (right panel of Figure 2) and higher ones do not provide an improvement that is worth the increase in computational time and storage.

The scheme of this procedure is shown in Figure 1. Step 1 follows the green arrow direction by interpolating the logarithm of the absorption coefficients over the logarithm of pressures. Step 2 follows the yellow arrow direction interpolating the fit coefficients from step 1 over the inverse of temperatures. Finally, step 3 follows the red arrow interpolating the fit coefficients from steps 2 over the mixing ratios.

The uncertainty between the exact CH_4 absorption coefficients computed with *P*=162 mbar, *T*=200 K, χ =0.001 and the interpolated ones is shown in Figure 2. In the whole spectral range considered for methane (870 nm – 6000 nm, left panel), the interpolation method from this work produces average uncertainties of about 5% (black line). By applying our method to different sets of the P,T and χ values given in Table 3 we verified that the above average errors represent an upper limit, demonstrating the reliability of the procedure. In the same range, the average uncertainties from Hill et al. (2013) interpolation method, adopted in the τ-REX RT tool (Waldmann et al., 2015), are about 35% (green line). As reference, the errors computed from the line intensity uncertainties given in the HITRAN database oscillate between 5% and 30% (orange line). The right panel of Figure 2 provides a zoom in the small range 870.00 nm – 870.05 nm to better show the uncertainties deriving from different interpolation methods.

T [K]	P [mbar]	χ
70	0.001	10^{-5}
100	0.006	10^{-4}
150	0.03	10^{-3}
200	0.2	1
250	1	
300	5	
350	30	
400	160	
450	900	
500	5000	

Table 3: values of *T* (panel A), *P* (panel B) and χ (panel C) adopted for the computations. All combinations of the

values in panels A, B and C have been considered.

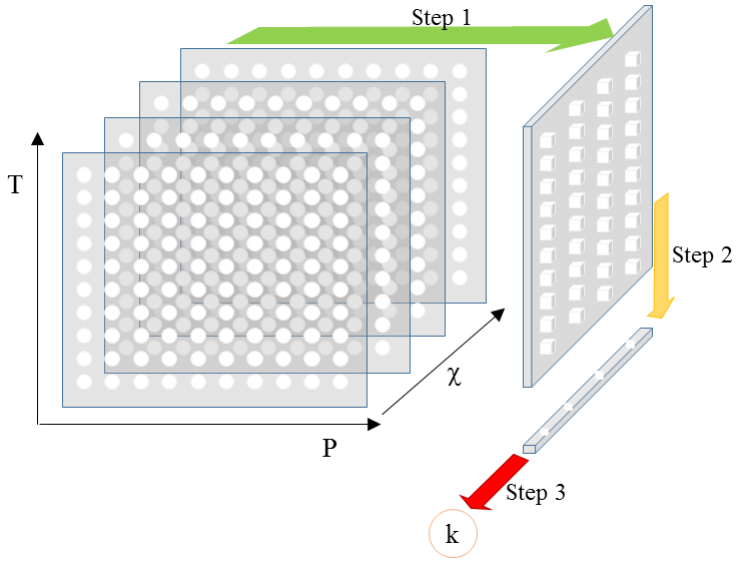

Figure 1: Representation in the space of the parameters of the 3-steps interpolation scheme described in Section 2.2 to obtain the absorption coefficients at the desired T and P for a given value of χ.

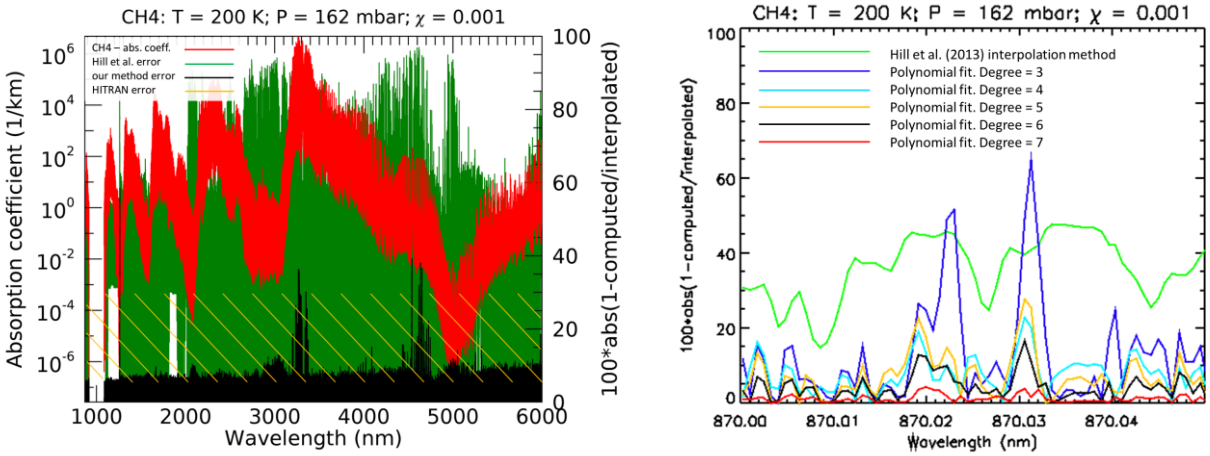

Figure 2: *At left*: relative differences (right axis) between CH_4 absorption coefficients computed with P = 162 mbar, T = 200 K, χ = 0.00.1 between 870 nm and 6000 nm (red line, left ordinate axis) and those interpolated with our method (black line) and with that from Hill et al. (2013) (green line). The orange oblique lines indicate the range of uncertainty due to HITRAN line intensity error (Section 2.1). *At right*: zoom in the range 870.00 nm – 870.05 nm of the relative differences between the computed absorption coefficients (left panel, red line) and the ones interpolated with polynomial fits of different degree: 3rd degree (blue line), 4th degree (cyan line), 5th degree (orange lines), 6th degree (black line) and 7th degree (red line). The relative difference obtained with Hill et al. (2013) interpolation method is shown in green.

3. Aerosols optical properties

3.1. Refractive indices data

Single scattering optical properties (SSOPs) were computed for the most common ices and aerosols found in the Solar System atmospheres taking advantage of the optical constants available in literature. The considered species are given in Table 4. Mars dust (Wolff et al., 2009), is mainly composed by nanophase ferric oxide particles (Morris et al., 2006; Poulet et al., 2007) and is produced by soil weathering (Pollack et al., 1979; Korablev et al., 2005), strongly affecting the planet's thermal structure and climate (Forget et al., 1999). Tholins (Khare et al., 1984; Cruikshank et al., 1993) are mixtures deriving from the photochemistry of molecular nitrogen and methane (N_2-CH_4) and are candidate to be the main component of Titan aerosols. H_2SO_4 clouds (Knollenberg & Hunten, 1980) dominate Venus cloud deck, likely of volcanic origins (Brackett et al., 1995). NH_3 and NH_4SH ices (Howett et al., 2007) are expected as condensed clouds on Jupiter and Saturn. CO_2 ice (Hansen et al., 2005) is known to condense in clouds in Martian atmosphere (Montmessin et al., 2007). HCN ice (Moore et al., 2010) is known to be a condensable species in Titan's atmosphere. H_2O ice (Mastrapa et al., 2008, 2009) is the most common ice in the Solar System.

Table 4: Summary of the solid/liquid species for which single scattering properties are calculated.

Species	T (K)	Particle effective radius		Spectral range		N_{max}
		$r_{min}(\mu m)$	$r_{max}(\mu m)$	$\lambda_{min}(nm)$	$\lambda_{max}(nm)$	
Mars dust *(Wolff et al., 2009)*	-	0.1	10	263	4994	917
N_2CH_4 Titan Tholin *(Khare et al., 1984)*	-	0.1	50	1842	5464	639
H_2SO_4	-	0.1	10	250	5494	950

(Knollenberg & Hunten, 1980)						
NH_3 ice *(Howett et al., 2007)*	80	0.1	20	840	5494	541
NH_4SH ice *(Howett et al., 2007)*	80; 160	1.0	100	833	5494	2493
H_2O ice *(Mastrapa et al., 2008,2009)*	80; 120	0.01	50	1111	5500	1076
CO_2 ice *(Hansen et al., 2005)*	-	0.01	10	252	5500	94
HCN ice *(Moore et al., 2010)*	95	0.1	10	2000	4033	117
Triton Tholin *(Cruikshank et al., 1993)*	-	0.1	50	258	740	4643

3.2. *Computation of scattering Look-Up tables*

In this section we describe the strategy adopted to produce and optimize the SSOPs LUTs. Firstly, the following assumptions were adopted:

- Particles are spherical: this assumption, relevant only for size parameter ($x=2\pi r/\lambda$) for which the Rayleigh approximation is no more valid, allows the adoption of the Mie theory for which well documented and relatively efficient software for the computation of SSOPs are available;
- Particles are homogeneous and only external mixing is allowed;
- Simulations are performed with a scalar RT Model. This assumption, that allows to represent the scattering matrix only with the description of the phase function, derives from the characteristics of the instruments for which the radiative transfer model is developed. These have very low sensitivity to the polarization of the measured radiances.

With the above assumptions, at a given wavelength, a single particle will be fully described by the value of its radius and of the two components of the complex refractive index. In terms of stored SSOPs the particle is characterized by the value of its extinction cross section, the single scattering albedo and a number of un-normalized coefficients for the Legendre polynomials. This approach has been preferred because most of the RT models require the Legendre coefficients as input for the phase function computation.

SSOPs were computed assuming spherical particles and taking advantage of the MIEV0 program (Wiscombe, 1980). Hence, the maximum extent of particle radius values was defined based on the limits of MIEV0 within the spectral range of interest, that is constrained in terms of size parameter. No attempt was done to estimate SSOP for size parameter values larger than the upper limit for which the validity of MIEV0 software was tested ($x = 20000$). On the opposite edge, Mie model has not been applied below the limit $x = 0.1$. In this case we tested several small-particles approximations (e.g. Penndorf 1962), finally adopting the Rayleigh one in the SSOP LUTs. It is worth noting that small-particles approximations represent a computationally efficient alternative to the Mie theory within their validity range, and in this case retrieval algorithms can better exploit a real-time evaluation of SSOP instead of resorting to LUTs. However, no attempt was done to optimize the computation of SSOP in the Rayleigh-Mie transition region ($0.1 \leq x \leq 2$).

From the above considerations, for a given species, the dimension of the stored LUTs will depend from the number of wavelengths, particles radii and Legendre coefficients.

For practical reasons, the approach of a fixed number of radii and maximum number of Legendre coefficients was adopted. SSOPs were computed for a set of 1366 values of radii ranging from 0.001 to 791.89 μm and each differing of 1% with respect to the previous value.

Since we have a fixed number of radii, the optimization of the size of the LUTs was based on the reduction of the number of wavelengths at which SSOPs are tabulated and on the definition of the minimum number of Legendre coefficients.

Reduction on the number of tabulated wavelengths was based on a two-step procedure. Firstly, we started from the shortest wavelength value in the range of interest, then we searched for the next wavelength value at which any of the two components of the complex refractive index differs more than 1%. This procedure is effective in reducing the number of wavelengths far from the resonances where the spectral variability of the refractive index is large. However, within the spectral range of resonances the above criterion is not so efficient and, hence, a second criterion has been adopted to further reduce the number of wavelengths. This test is similar to the first one (a threshold of 0.1% is adopted this time) except that for the SSOP is based on the differences, computed over the whole set of radii, between extinction coefficients and single scattering albedo values at different tabulated wavelengths. Note that, the adopted criterion adopted allows the use of the smaller tabulated wavelength in the computation without need of interpolation.

For some species, the wavelength range for which tabulated values of the complex refractive index are available does not cover the overall range of wavelengths of interest considered in this study. No attempt was done to extend the original range for example with extrapolation of the values through a functional fit. We discarded this possibility because of the high level of uncertainty in the extrapolation process and the high sensitivity to the fitting procedure adopted (functional form and fitted dataset).

Compared to the most common way to implement LUTs for aerosols scattering, we stored single particle optical properties rather than values computed for polydispersions for which a distribution of sizes is taken into account (e.g. Hess et al. 1998). This has been done in order to allow the computation for any possible size distribution. From the point of view of inversion algorithms, this choice results in more flexibility for choice of retrievable quantities, allowing the retrieval of the size distribution itself. A direct consequence of storing single particles SSOPs is the need of a larger number of Legendre coefficients to correctly represent the phase matrix elements. For example, Figure 3 shows the results of 4 different parameterizations available in literature estimating the minimum number of required Legendre coefficients as a function of the size parameter x, including the one adopted in MIEV0. It is evident that large x values (i.e. for large radii and short wavelengths) require more than 10000 Legendre expansion terms. However, these parameterizations do not take into account the value of the complex refractive index. For example, large values of the imaginary part result in a smoother phase function and, therefore, a smaller number of Legendre coefficients is required.

The number of Legendre coefficients can be truncated with methods like the δ-M (Wiscombe, 1977) or others (Nakajima and Tanaka 1988; Hu et al. 2000; Mitrescu and Stephens 2004; Lin et al., 2018; for a review see Sharma 2015) that, however, are usually applied to integrated polydispersions. For example, in the widely used DISORT2 solver (Stamnes et al., 2000) the δ-M is automatically adopted consistently with the input characteristics of the required simulation.

Since for the above reasons, these methods are not suitable for our LUTs, we perform an optimization on the number of Legendre coefficients based on the phase functions reconstruction for polydispersions, for which less coefficients are required.

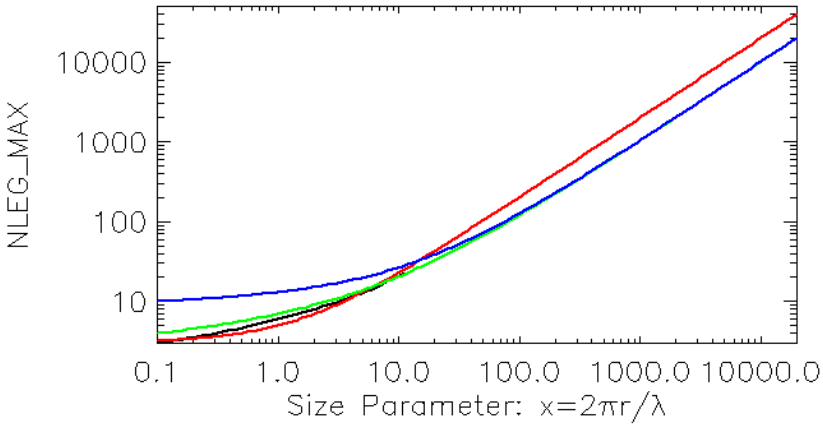

Figure 3: Minimum number of Legendre coefficients required to describe the phase function of a single homogeneous spherical particle of HCN ice, computed according to Wiscombe (1980) (Black), Lenoble (1993) (Red), Bohren and Huffman (1983) (Green) and Mishchenko et al (2002) (Blue).

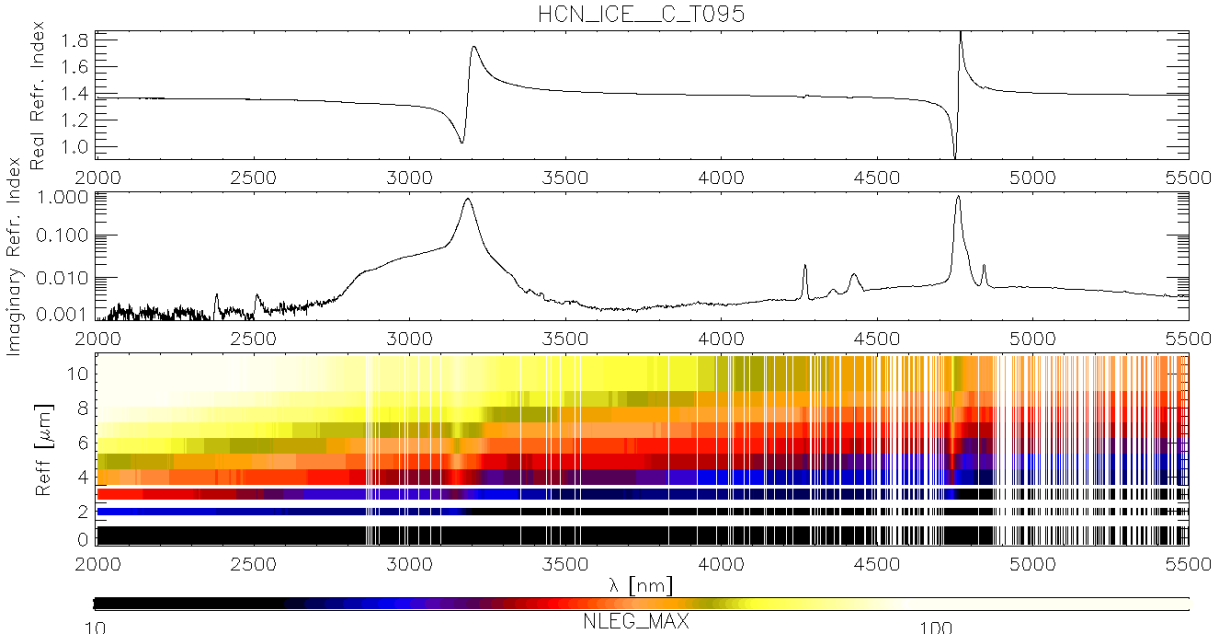

Figure 4: *Top and middle panels*: real and imaginary parts of HCN ice refractive index. *Lower panel:* Minimum number of Legendre coefficients required to describe the phase function of a lognormal size distribution of spherical particles with v_{eff} = 0.3 computed according to Wiscombe (1980). Blank regions represent wavelengths and radii removed after the optimization process (see Section 3.2).

There is no general parameterization for the choice of the number of Legendre coefficients for polydispersions. For example, Ding et al. (2009) found that a maximum of 32 Legendre coefficients are required to represent ice and water clouds (16 for dust aerosols). But, besides the fact that this low number is obtained after applying the δ-fit method (Hu et al, 2000) to the original SSOPs, they found that truncated phase functions cannot match perfectly the original counterparts at some scattering angles. This is evident, for example, in the rainbow region for a water cloud and sharply peaked halos for an ice cloud. On the other hand, Kokhanosky et al (2010) used up to 720 Legendre expansion terms, while Rozanov and Lyapustin (2010) found a value of 680 depending on the code, the wavelength and the microphysics of the polydispersion (water cloud vs aerosols). An example

of the dependence of the minimum number of Legendre coefficients with the particles effective radius (r_{eff}) and wavelength for a lognormal size distribution (Hansen and Trevis, 1974) of HCN particles is given in Figure 4.

For the above reasons, a species- and size distribution-dependent procedure to define the minimum number of coefficients was developed to optimize the LUTs. The optimization procedure was based on the comparison of the computed phase functions for a set of size distributions. We evaluated that Legendre polynomials of orders greater than 5000 contribute less than 10^{-3} to the phase function reconstruction for all the species and wavelengths in Table 3. Then we iteratively decreased the number of Legendre coefficients until the average percentage difference between the initial and the current phase function, computed over 181 regularly spaced scattering angles in the entire range (0°-180°), is larger than 1%.

For the above optimization procedure, the log-normal functional form has been assumed as size distribution, being one of the most commonly adopted to perform RT studies of planetary atmospheres. This distribution is parameterized with the particles modal radius (r_g) and standard deviation (σ_g) (Hansen and Trevis, 1974). We computed r_g and σ_g from a discretized set of r_{eff} and effective variances (ν_{eff}) (Hansen and Trevis, 1974), since these are the quantities that are usually compared in RT studies of planetary atmospheres. The ranges of effective radii considered to generate the size distributions depend from the species and their value is reported in Table 4. Such ranges are defined to ensure that the LUT is suitable to study the different atmospheres of the Solar System planets. To generate a set of size distributions the overall r_{eff} range (0.01-100 μm) was discretized by defining 10 equally spaced values for each order of magnitude for a total of 37 values. For the effective variances (ν_{eff}) we considered for all species the values ν_{eff} = 0.1, 0.2, 0.3, 0.4 and 0.5 μm, ranging from the minimum to the maximum values found in literature (Ramirez-Beltran et al., 2009; Karkoschka & Tomasko, 2005; Roman et al., 2013; Millour et al., 2015). With the above assumptions for a given species, up to 185 size distributions are used in the Legendre coefficients optimization. Note that a similar approach also includes unrealistic size distributions such as the one with very large r_{eff} and small ν_{eff}. More realistic size distribution are probably obtained with effective variance values proportional to the effective radius one (e.g. Gavrilova & Ivlev 1996). However, as expected these size distributions characterized by large r_{eff} and relatively small v_{eff} are the ones that require the largest number of coefficients. Therefore, even if probably less representative of real polydispersions in planetary atmospheres, the set generated was used to obtain a conservative estimation of the number of Legendre coefficients required to reliably represent the phase functions (see Table 4). The obtained values range roughly from 100 to about 4600. As expected, the latter value is needed for wavelengths in the UV range for polydispersions with a large r_{eff} and intermediate v_{eff} and for species with relatively high real component of the refractive index and corresponding low value for the imaginary part (Figure 4).

Regarding the use of a large number of Legendre coefficients in numerical simulations, it should be noted that, in previous versions of multiple scattering RT solvers (e.g. Stamnes et al 1988, Evans and Stephens 1991) the number of Legendre coefficients was proportional to the number of streams for the simulation, increasing drastically the computational needs. However, this is no longer valid for recent solvers (e.g. Lin et al. 2015) as well as for Monte Carlo based ones.

4. Computational time improvement and LUTs application to planetary data

The improvement in terms of computational time for using the LUTs with respect to the dynamic computation of aerosols and gases properties every time they are needed has been tested on a PC

equipped with an Intel Core i5 CPU650 with a 3.2 GHz frequency and 3.8 Gb of system RAM. The real-time computation of the scattering properties of a polydispersion of H_2O ice at 80 K in the wavelength range 1111 nm – 5500 nm considering more than 3000 spectral points (the procedure adopted to resize the spectral grids is described in Section 3.2), is performed in about 80 minutes while just a few seconds are required to read the SSOPs LUTs. Similarly, the computation of the absorption coefficients of CH_4 considering the wavelength range and resolutions provided in Table 2 requires 14 minutes for a single set of P,T and χ (i.e. for a single atmospheric layer). On the other hand, the reconstruction of the same absorption coefficients using the GACs LUTs is performed in less than 1 minute.

For the reasons above, the advantage in using the LUTs with respect to the real-time computation is evident. The application of the LUTs to RT computations has been tested for case studies on Saturn, Mars and Jupiter.

In the case of Saturn, we exploited the GAC LUTs for CH_4 to model VIMS data in the 1.5 – 4.0 μm wavelength range observing a faint luminescent ring in the northern polar cap of the planet (Adriani et al., 2015).

Jupiter data in the range 2.4 – 3.0 μm from the JIRAM spectrometer have been analyzed taking advantage of CH_4 and H_2O GAC LUTs, and tholin and NH_3 SSOPs LUTs (Sindoni et al., 2017).

CO_2 and H_2O GAC LUTs have been used together with the Mars dust SSOP LUT to study a Martian local storm in the range 0.5 – 2.5 μm observed by the OMEGA spectrometer (Oliva et al., 2018). Moreover, the same LUTs are being exploited to study OMEGA limb data in the same wavelength range.

5. Summary and future developments

We have described a database for gaseous and aerosols optical properties in the VIS-NIR spectral range (400-5500 nm) for some of the main components of planetary atmospheres. We focused on CH_4, CO_2, and H_2O molecular species for gaseous absorption, and on the scattering properties of condensates likely forming the bulk of atmospheric particulates (Table 4). This database is valuable as input for RT calculations especially for the atmospheres of Venus, Mars, Jupiter, Saturn, and Titan. Gaseous coefficients have been computed with the LBL approach adopting Voigt line shapes for several combinations of pressures, temperatures and mixing ratios suitable to describe the atmospheres of rocky and gaseous planetary environment. A new interpolation method tested on these LUTs is suggested for obtaining absorption coefficients for the desired values of P, T and χ with improved accuracy.

On the other hand, for the SSOPs of the species of interest, we assumed homogeneous spheres to compute the LUTs for single particles. Mie theory has been adopted within the limit $0.1 < x < 20000$ and Rayleigh for particles with $x < 0.1$. Within the LUTs we provide the Legendre coefficients of phase functions, in a number sufficient to accurately describe the considered radii polydispersions within the ranges given in Table 4.

The LUTs discussed here must be thought as forming a first version of the database. Several developments are foreseen in the next future. The gaseous line parameters will be extended to include the recently distributed HITRAN 2016 version (Gordon et al., 2017). Further molecules, such as CO, NH_3, PH_3, that are present in many atmospheres as trace gases, will be processed and inserted in the database. Moreover, we will evaluate the possibility to produce LUTs with different line shapes/broadenings and we will extend temperature, pressure and mixing ratio ranges to account for the most extreme environments in the Solar Sytem.

We plan analogous upgrades for the SSOPs LUTs, with the inclusion of other species, like hydrocarbon ices, polycyclic aromatic hydrocarbons (PAH) and mixtures. The inclusion of non-spherical and coated particles, expected to be present in the outer Solar System, will be evaluated to account for different microphysical regimes.

Acknowledgements

This study has been funded within the PRIN INAF 2014 project. We would like to thank Marco Giardino, Sergio Fonte and Romolo Politi, for the precious help they provided in the management of the HPC machines and their support within the HPP and DataWell facilities at INAF-IAPS.

References

Adriani, A. et al., 2015. "Faint Luminescent Ring over Saturn's Polar Hexagon", Astrophys. J. Lett., 808, L16.

Adriani, A., et al., 2017. "JIRAM, the Jovian Infrared Auroral Mapper", Sp. Sci. Rev., 213, 393, 2017.

Bohren, C. F and Huffman, D. R, (1983) "Absorption and scattering of light by small particles", New York: Wiley, 1983.

Brackett, R.A. et al., 1995. Volatile transport on Venus and implications for surface geochemistry and geology. Journal of Geophysical Research, Vol. 100, n. E1, pp. 1553-1563.

Brown, R. H., Baines, K. H., Bellucci, G., et al. (2004). "The Cassini visual and infrared mapping spectrometer (VIMS) investigation". Space Sci. Rev. 115, 118–168.

Brown, A. J., Piqueux, S., Titus, T. N. (2014). " Interannual observations and quantification of summertime H2O ice deposition on the Martian CO2 ice south polar cap", Earth and Planetary Science Letters, Volume 406, p. 102-109.

Buehler, S.A. et al., 2011. Absorption lookup tables in the radiative transfer model ARTS, Journal of Quantitative Spectroscopy & Radiative Transfer 112, 1559–1567.

Cess, R.D. and Ramanathan, V., 1972. Radiative Transfer in the Atmosphere of Mars and that of Venus above the cloud deck. J. Quant. Spectrosc. Radiat. Transfer 12, 933-945.

Chance, K. and Martin, R.V., 2017. Spectroscopy and Radiative Transfer of Planetary Atmospheres 1st Edition. Oxford University Press; 1 edition (May 23, 2017).

Colaprete, A. and Toon, O.B., 2000. The Radiative Effects of Martian Water Ice Clouds on the Local Atmospheric Temperature Profile. Icarus 145, 524–532.

Cruikshank, D.P., et al., 1993. "Ices on the surface of Triton". Science, vol. 261, no. 5122, p. 742-745.

Ding,S., Y. Xie, P.Yang, F.Weng, Q.Liu, B.Baum, Y. Hu, Estimates of radiation over clouds and dust aerosols: Optimized number of terms in phase function expansion, J. Quant. Spectrosc. Radiat. Transfer,110, 13, 2009, 1190-1198.

Evans, K. F. and Stephens, G. L. (1991). A new polarized atmospheric radiative transfer model, Journal of Quantitative Spectroscopy and Radiative Transfer (ISSN 0022-4073), vol. 46, Nov. 1991, p. 413-423.

Fletcher, L.N., et al., 2015. Seasonal evolution of Saturn's polar temperatures and composition. Icarus 250, 131–153.

Fletcher, L.N. , Orton, G.S. , Teanby, N.A. , et al. , 2009. Methane and its isotopologues on Saturn from Cassini/CIRS observations. Icarus 199, 351–367.

Forget, F., Hourdin, F., Fournier, R., Hourdin, C., Talagrand, O., Collins, M., Lewis, S.R., Read, P.L., Hout, J.-P, 1999. Improved general circulation models of the Martian atmosphere from the surface to above 80 km. J. Geophys. Res. 104, 24,155–24,176.

Gavrilova, L.A. , Ivlev, L.S. , 1996. Aerosol models for computations of radiative characteristics of the atmosphere. Atmos. Oceanic Phys. 31 (5), 638–649.

Geminale, A., Grassi, D., Altieri, F., Serventi, G., Carli, C., Carrozzo, F. G., Sgavetti, M., Orosei, R., D'Aversa, E., Bellucci, G., Frigeri, A. (2015). "Removal of atmospheric features in nir spectra by means of PCA and Target Transformation on Mars - I.Method ", Icarus,253,51.

Goody R.M., Young Y. (1989). "Atmospheric Radiation: Theoretical Basis". Oxford University Press: New York.

Goody, R.M., 1952. A statistical model for water vapor absorption. Q. J. R. Meteorol. Soc. 78, pp. 165–9.

Gordon, I.E., et al., 2017. The HITRAN2016 molecular spectroscopic database. Journal of Quantitative Spectroscopy & Radiative Transfer, 203, 3-69.

Hill, C., et al., 2013. Temperature-dependent molecular absorption cross sections for exoplanets and other atmospheres. Icarus, 226, 1673-1677.

Hansen, G.B, 2005. "Ultraviolet to near-infrared absorption spectrum of carbon dioxide ice from 0.174 to 1.8 μ m", Journal of Geophysical Research, Volume 110, Issue E11, CiteID E11003.

Hansen, J. E. and Trevis L. D. (1974). "Light scattering in planetary atmospheres", Space Science Reviews, 16, 527.

Haus, R. and Arnold, G., 2010. Radiative transfer in the atmosphere of Venus and application to surface

emissivity retrieval from VIRTIS/VEX measurements. Planetary and Space Science 58, 1578–1598.

Hess, M., Koepke, P., Schult, I. (1998). "Optical Properties of Aerosols and Clouds: The Software Package OPAC", Bulletin of the American Meteorological Society, 79, 831.

Howett, C.J.A., et al., 2007. "*Optical constants of ammonium hydrosulfide ice and ammonia ice*". J. Opt. Soc. Am. B/Vol. 24, No. 1, 126-136.

Hu, Y.-X., Wielicki, B., Lin, B., Gibson, G., Tsay, S.-C., Stamnes, K., Wong, T. (2000). "δ-fit- A fast and accurate treatment of particle scattering phase functions with weighted singular-value decomposition least-squares fitting", JQRST,65,681.

Ignatiev, N.I., Grassi, D., Zasova, L.V., 2005. Planetary Fourier spectrometer data analysis: fast radiative transfer models. Planet. Space Sci. 53 (10), 1035–1042.

Irwin, P., et al., 2008. The NEMESIS planetary atmosphere radiative transfer and retrieval tool. J. Quant. Spectrosc. Radiat. Transf. 109 (6), 1136–1150.

Karkoschka, E. and Tomasko, M., 2005. "Saturn's vertical and latitudinal cloud structure 1991-2004 from HST imaging in 30 filters", Icarus, Volume 179, Issue 1, p. 195-221.

Karkoschka, E. , Tomasko, M.G. , 2010. Methane absorption coefficients for the jovian planets from laboratory, Huygens, and HST data. Icarus 205, 674–694 .

Khare, B.N. et al., 1984. "Optical constants of organic tholins produced in a simulated Titanian atmosphere - From soft X-ray to microwave frequencies". Icarus, 60, 127-137.

Kokhanovsky, A. A., Budak, V. P., Cornet, C., Duan, M., Emde, C., Katsev, I. L., Klyukov, D. A., Korkin, S. V., Labonnote , L., Mayer, B., Min, Q., Nakajima, T., Ota, Y., Prikhach, A. S., Rozanov, V. V., Yokota, T., Zege, E. P. (2010). "Benchmark results in vector atmospheric radiative transfer", JQSRT, 111, pp.1931-1946.

Korablev, O., Moroz, V. I., Petrova, E. V., Rodin, A. V. (2005). "Optical properties of dust and the opacity of the Martian atmosphere", Advances in Space Research, Volume 35, Issue 1, p. 21-30.

Knollenberg, R. G. and Hunten, D. M. (1980). "The microphysics of the clouds of Venus - Results of the Pioneer Venus particle size spectrometer experiment", Journal of Geophysical Research, vol. 85, Dec. 30, 1980, p. 8039-8058.

Lenoble, J. (1993). "Atmospheric radiative transfer", Studies in Geophysical Optics and Remote Sensing, Hampton, VA: A. Deepak Pub., 1993.

Lin, Z., Stamnes, S., Jin, Z., Laszlo, I., Tsay, S.-C., Wiscombe, W., Stamnes, K. (2015). "Improved discrete ordinate solutions in the presence of an anisotropically reflecting lower boundary: Upgrades of the DISORT computational tool". J. Quant. Spectrosc. Radiat. Transfer, 157, 119–134.

Lin, Z., N. Chen, Y. Fan, W. Li, K. Stamnes, and S. Stamnes, 2018: New Treatment of Strongly Anisotropic Scattering Phase Functions: The Delta-M+ Method. *J. Atmos. Sci.*, **75**, 327–336.

Mastrapa, R.M. et al., 2008. "Optical constants of amorphous and crystalline H2O-ice in the near infrared from 1.1 to 2.6 μm". Icarus, Volume 197, Issue 1, 307-320.

Mastrapa, R.M. et al., 2009. "Optical Constants of Amorphous and Crystalline H2O-ice: 2.5-22 μm (4000-455 cm-1) Optical Constants of H2O-ice". The Astrophysical Journal, Volume 701, Issue 2, pp. 1347-1356.

Millour, E., et al., 2015. "The Mars Climate Database (MCD version 5.2)", European Planetary Science Congress 2015, held 27 September - 2 October, 2015 in Nantes, France.

Mishchenko, M. I., Travis, L. D., Andrew, L. A. (2002). "Scattering, absorption, and emission of light by small particles", Cambridge University Press, 2002.

Montmessin, F., Gondet, B., Bibring, J.-P, Langevin, Y., Drossart, P., Forget, F. and Fouchet, T., 2007. Hyperspectral imaging of convective CO2 ice clouds in the equatorial mesosphere of Mars. Journal Of Geophysical Research, Vol. 112, E11S90.

Mitrescu, C., Stephens, G. L. (2004). "On similarity and scaling of the radiative transfer equation", Journal of Quantitative Spectroscopy and Radiative Transfer, Volume 86, Issue 4, 15 July 2004, Pages 387-394.

Moore, M.H. et al., 2010. "Infrared Spectra and Optical Constants of Nitrile Ices Relevant to Titan's Atmosphere". The Astrophysical Journal Supplement, Volume 191, Issue 1, pp. 96-112.

Morris, R. V., Klingelhöfer, G., Schröder, C., Rodionov, D. S., Yen, A., Ming, D. W., de Souza, P. A., Fleischer, I., Wdowiak, T., Gellert, R., Bernhardt, B., Evlanov, E. N., Zubkov, B., Foh, J., Bonnes, U., Kankeleit, E., Gütlich, P., Renz, F., Squyres, S. W., Arvidson, R. E. (2006). "Mössbauer mineralogy of rock, soil, and dust at Gusev crater, Mars: Spirit's journey through weakly altered olivine basalt on

the plains and pervasively altered basalt in the Columbia Hills", Journal of Geophysical Research, Volume 111, Issue E2, CiteID E02S13.

Nakajima, T. and Tanaka, M. (1988). "Algorithms for radiative intensity calculations in moderately thick atmospheres using a truncation approximation", Journal of Quantitative Spectroscopy and Radiative Transfer, vol. 40, July 1988, p. 51-69.

Oliva, F. et al., 2016. "Clouds and hazes vertical structure of a Saturn's giant vortex from Cassini/VIMS-V data analysis", Icarus, Volume 278, 215.

Oliva, F. et al., 2018. "Properties of a Martian local dust storm in Atlantis Chaos from OMEGA/MEX data", Icarus, 300, 1.

Penndorf, R. (1962). "Approximation Formula for Forward Scattering," J. Opt. Soc. Am. 52, 797-799.

Pérez-Hoyos, S., et al., 2005. Saturn's cloud structure and temporal evolution from ten years of Hubble Space Telescope images (1994–2003). Icarus 176, 155–174.

Pérez-Hoyos, S., et al., 2012. The 2009–2010 fade of Jupiter's South Equatorial Belt: Vertical cloud structure models and zonal winds from visible imaging. Icarus 217, 256–271.

Piccioni, G., et al., 2007. VIRTIS: The Visible and Infrared Thermal Imaging Spectrometer. ESA Special Publication, SP-1295, 1-27.

Piccioni, G., et al., 2014. MAJIS, the Moons And Jupiter Imaging Spectrometer, designed for the future ESA/JUICE mission. Geophysical Research Abstracts Vol. 16, EGU2014-10925-2.

Pierrot, L., A.Soufiani, J.Taine,1999, Accuracy of narrow-band and global models for radiative transfer in H_2O, CO_2, and H_2O-CO_2 mixtures at high temperature", JQSRT, Volume 62, Issue 5, July 1999, Pages 523-548.

Pollack, J. B.; Colburn, D. S.; Flasar, F. M.; Kahn, R.; Carlston, C. E.; Pidek, D. G. (1979). "Properties and effects of dust particles suspended in the Martian atmosphere", Journal of Geophysical Research, vol. 84, June 10, 1979, p. 2929-2945.

Poulet, F., et al., 2003. Compositions of Saturn's rings A, B, and C from high resolution near-infrared spectroscopic observations. Astronomy & Astrophysics 412, 305–316.

Poulet, F.; Gomez, C.; Bibring, J.-P.; Langevin, Y.; Gondet, B.; Pinet, P.; Belluci, G.; Mustard, J. (2007). "Martian surface mineralogy from Observatoire pour la Minéralogie, l'Eau, les Glaces et l'Activité on board the Mars Express spacecraft (OMEGA/MEx): Global mineral maps", Journal of Geophysical Research, Volume 112, Issue E8, CiteID E08S02.

Ramirez-Beltran, N. D., Kuligowsky, R. J., Cardona, M. J., et al. (2009). "Warm rainy clouds and droplet size distribution". Wseas Trans. Syst. 8 (1), 75–85.

Roman, M. T., Banfield, D., Gierasch, P. J. (2013). "Saturn's cloud structure inferred from Cassini ISS", Icarus, Volume 225, Issue 1, p. 93-110.

Rothman, L. S., Rinsland, C. P., Goldman, A. et al., "The HITRAN Molecular Spectroscopic Database and HAWKS (HITRAN Atmospheric Workstation): 1996 Edition", *Journal Of Quantitative Spectroscopy and Radiative Transfer* **60**, 665-710 (1998)

Rothman, L. S., Gordon, I. E., Babikov, Y., et al. , 2013. The HITRAN2012 molecular spectroscopic database. J. Quant. Spectrosc. Radiat. Trans. 130, 4–50.

Rozanov V.V., Lyapustin A.I., (2010). "Similarity of radiative transfer equation: Error analysis of phase function truncation techniques", JQSRT, 111, pp.1964 – 1979.

Sharma, S.K. 2015, A review of approximate analytic light-scattering phase functions. In: A. Kokhanovsky (ed.), Light Scattering Reviews 9, Springer Praxis Books. pp.53-100

614 Sindoni, G. et al., 2017. “Characterization of the white ovals on Jupiter's southern hemisphere using the first
615 data by the Juno/JIRAM instrument”, Geophys. Res. Lett., 44, 4660.
616
617 Sromovsky, L.A., et al., 2013. Saturn’s Great Storm of 2010–2011: Evidence for ammonia and water ices
618 from analysis of VIMS spectra. Icarus 226, 402–418.
619 Stamnes, K., et al., 1988. “Numerically stable algorithm for discrete-ordinate-method radiative transfer in
620 multiple scattering and emitting layered media”. Appl. Opt. 27 (12), 2502–2509.
621 Stamnes, K. (2000). “DISORT, a general-purpose Fortran program for Discrete-Ordinate-Method Radiative
622 Transfer in Scattering and Emitting Layered Media: documentation and methodology”, DISORT
623 Report v1.1.
624 Titov, D.V. et a., 2007. Radiation in the atmosphere of Venus. Exploring Venus as a Terrestrial Planet.
625 (2007), Geophys. Monogr. Ser., vol. 176, edited by L. W. Esposito, E. R. Stofan, and T. E. Cravens,
626 pp. 121-138, AGU, Washington, D. C.
627
628 Vincent, R.A. and Dudhia, A., 2017. Fast radiative transfer using monochromatic look-up tables. Journal of
629 Quantitative Spectroscopy & Radiative Transfer 186, 254–264.
630 Wiscombe, W.J., 1977. The Delta-M method: rapid yet Accurate radiative flux calcutions for strongly
631 asymmetric phase functions. Journal of the atmospheric sciences, Vol. 34, 1408 – 1422.
632 Wiscombe, W.J., 1980. “Improved Mie scattering algorithms”, Appl.Opt.19,1505.
633 Waldmann, I.P., et al., 2015. Tau-REx I: A next generation retrieval code for exoplanetary atmospheres. The
634 Astrophysical Journal, 802:107, 18pp.
635 West, R., et al., 2010. The correlated-k method and related methods for broadband radiation calculations.
636
637 Wolff, M.J., et al., 2009. “Wavelength dependence of dust aerosol single scattering albedo as observed by
638 the Compact Reconnaissance Imaging Spectrometer”. J. Geophys. Res. 114 (E9).
639
640 Zhang, X. et al., 2013. Stratospheric aerosols on Jupiter from Cassini observations. Icarus 226, 159–171.
641